Magnetic field enhanced zero-bias conductance in vertical Josephson junctions based on Weyl semimetals

Zhu Lin,[1,2] Hua-Ding Song,[1] Xing-Guo Ye,[1] Jianhong Xue,[3] An-Qi Wang,[1] Yan Zhang,[1] Song Liu,[2] Zhensheng Zhang,[2] Hongqi Xu,[3] Dapeng Yu,[2] and Zhi-Min Liao[1,3,4,*]

[1]*State Key Laboratory for Mesoscopic Physics and Frontiers Science Center for Nano-optoelectronics, School of Physics, Peking University, Beijing 100871, China*

[2]*Institute for Quantum Science and Engineering and Department of Physics, Southern University of Science and Technology, Shenzhen 518055, China*

[3]*Beijing Key Laboratory of Quantum Devices, Peking University, Beijing 100871, China*

[4]*Collaborative Innovation Center of Quantum Matter, Peking University, Beijing 100871, China*

(Received 17 September 2019; revised manuscript received 5 June 2020; accepted 8 June 2020; published 22 June 2020)

We report the magnetotransport properties of T_d-$MoTe_2$ based vertical junctions with NbN superconducting electrodes. Benefiting from the high critical magnetic field of NbN, the superconducting state is maintained up to 8 T. A sharp drop of resistance is observed at $T_c \sim 13$ K, corresponding to the critical temperature of NbN electrodes. The differential conductance spectra show that the zero-bias conductance is increased by magnetic fields with 41.6% increment at 14 T. Intriguingly, negative magnetoresistance (MR) $\sim -48\%$ is observed under 8 T at 3 K. The negative MR disappears above superconductivity critical temperature $\sim$13 K. The Weyl semimetal $MoTe_2$ combined with superconductor is promising for searching topological superconductivity and Majorana zero modes.

DOI: 10.1103/PhysRevB.101.214519

I. INTRODUCTION

The layered transition-metal dichalcogenide materials have attracted continued interests owing to their unique physical properties [1–15]. Recently, $MoTe_2$ with orthorhombic T_d phase was confirmed as a type-II Weyl semimetal, where Weyl fermions emerge at the touching points of hole and electron pockets with breaking Lorentz invariance [6–11]. The type-II Weyl points are connected by topologically protected Fermi-arc surface states [10], which is a nontrivial feature of this topological material. T_d-$MoTe_2$ is also a promising platform for searching topological superconductivity [12–15]. An intrinsic superconducting transition is observed in bulk T_d-$MoTe_2$ at a critical temperature $\sim$0.1 K [13], which is believed to possess a nontrivial $s_\pm$ pairing mechanism [14–16]. Meanwhile, the superconductivity in T_d-$MoTe_2$ can also be induced through the proximity effect. It is proposed that the proximity effect may be localized near the superconductor-T_d-$MoTe_2$ interface [15,17] due to the layered nature and topological properties of T_d-$MoTe_2$. The combination of topology and superconductivity is believed to facilitate the progress of quantum computation [18–20]. However, the relationship between superconductivity and topological properties of T_d-$MoTe_2$ is still indistinct.

To study the interplay between superconductivity and T_d-$MoTe_2$, we fabricated the NbN/T_d-$MoTe_2$/NbN vertical junctions. The NbN superconducting electrodes are chosen due to the advantages of a relatively high critical temperature ($\sim$15 K) [21–23] and large upper critical field ($\sim$25 T) [22]. The ultrahigh critical field enables the investigations on Weyl semimetal/superconductor interfaces under large magnetic field, which has been utilized to induce topological superconducting phase in spin-orbit coupled nanowires [18–20]. By applying the magnetic field, topological transport features like the Adler-Bell-Jackiw (ABJ) anomaly of the Weyl fermions may emerge together with superconducting states at the surface.

In this work, the magnetoresistance (MR) behaviors, differential conductance spectra (dI/dV) and current-voltage (I-V) characteristics of the vertical junctions at low temperatures are investigated. Residual resistance is observed as the system is in the superconducting state, indicating the low transparency at interfaces between superconductors and $MoTe_2$. An evident negative MR behavior is observed up to 8 T, as the system is in the superconducting regime and within low bias. The dI/dV spectra show that the zero-bias conductance is enhanced by magnetic fields. Our findings will motivate further research on topological superconductors in type-II Weyl semimetals.

II. METHOD

The NbN-$MoTe_2$-NbN vertical junctions with cross-bar configuration were fabricated. The few-layer $1T'$-$MoTe_2$ flakes were mechanically exfoliated from bulk $MoTe_2$ crystal onto SiO_2/Si wafers. The room-temperature Raman spectrum [Fig. 1(a)] indicates two characteristic vibrational modes A_g and B_g of $1T'$-$MoTe_2$ [9–11]. The T_d-phase $MoTe_2$, a

*liaozm@pku.edu.cn

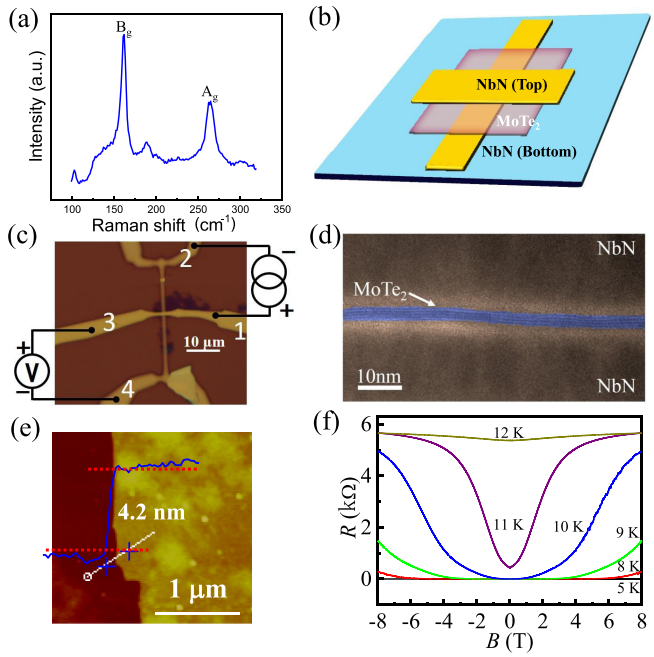

FIG. 1. (a) Room-temperature Raman spectrum of the few-layer $1T'$-$MoTe_2$ flake. Vibrational modes at $\sim$160 cm^{-1} (B_g) and $\sim$260 cm^{-1} (A_g) are detected. (b) Schematic diagram for a vertical NbN-$MoTe_2$-NbN junction device with cross-bar configuration. The top and bottom NbN superconducting electrodes sandwich the $MoTe_2$ flake. (c) A typical optical image of a NbN-$MoTe_2$-NbN vertical junction device. The terminals 1 and 3 are the top electrodes, and the terminals 2 and 4 are the bottom electrodes. Bias current is applied between terminals 1 and 2, and voltage is measured using terminals 3 and 4. (d) The TEM image (false color) of the cross section of the junction. The thickness of the $MoTe_2$ layer is $\sim$4 nm. (e) Atomic force microscopy image of the $MoTe_2$ flake. The height profile is carried out along the white dashed line between the positions labeled by the crosshairs. The thickness of the flake is $\sim$4.2 nm. (f) The resistance of the bottom NbN electrode as a function of magnetic field at various temperatures. At 5 K, the critical magnetic field is higher than 8 T.

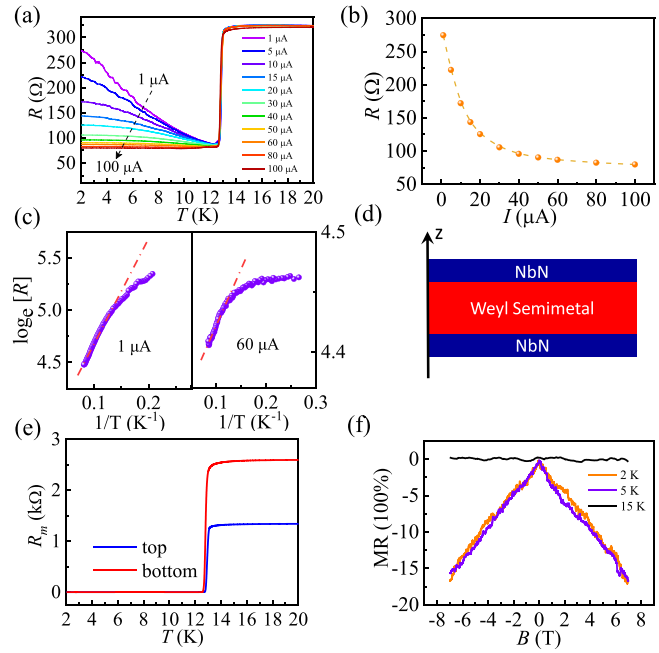

FIG. 2. (a) Temperature dependence of junction resistance (R) of device A measured by a four-probe crossbar configuration. A sharp drop of R occurs at $\sim$13 K with a residual resistance. The residual resistance is reduced by applying larger bias current. (b) The R as a function of applied current at temperature of 2 K. (c) The Arrhenius plots of ln$R$ vs $1/T$ for $I = 1$ and 60 μA, and the transport barrier height $\Delta_b = 0.87$ and 0.082 meV is obtained from the fittings, respectively. (d) Schematic of the NbN-$MoTe_2$-NbN vertical junction structure below T_c. (e) The resistance of top/bottom NbN electrodes (R_m) as a function of temperature. (f) Negative MR with $\sim -16\%$ under 8 T at temperatures of 2 and 5 K. The MR is about zero at 15 K.

type-II Weyl semimetal [10,11], is obtained from $1T'$-$MoTe_2$ after a structural phase transition at $\sim$250 K [9–11]. The selected high quality $MoTe_2$ flake was then transferred onto the prefabricated NbN electrodes (20 nm in thickness) on another Si/SiO_2 substrate by a dry transfer technique [24]. Then top NbN electrodes with thickness of 40 nm were fabricated on the flake to form a sandwiched cross-bar structure with the bottom NbN electrodes. Figure 1(b) shows the diagram of the vertical junction device. The optical image of a typical device is shown in Fig. 1(c), where bias current pass through the junction between terminals 1 and 2, and the voltage difference across the junction is measured using terminals 3 and 4. Figure 1(d) shows a transmission electron microscope (TEM) image of the cross section of the junction. The thickness of the $MoTe_2$ layer was measured to be $\sim$4 nm, consistent with the results of AFM [Fig. 1(e)]. The NbN superconducting electrodes exhibit vanishing resistance even with magnetic field up to 8 T at temperature of 5 K [Fig. 1(f)].

III. RESULTS

Figure 2(a) shows the temperature dependence of the junction resistance (R) of an NbN/$MoTe_2$/NbN vertical junction (device A) with different bias currents. The resistance at high temperatures are insensitive to the current intensity and temperature. A sharp drop of R is detected at $T_c \sim 13$ K, corresponding to the critical temperature of NbN electrodes [25–27]. There is a residual resistance $\sim$70 Ω after the transition, and it increases with decreasing temperature for 12 to 7 K [Fig. 2(a)]. When temperature goes down below 4 K, R becomes steady for bias current $I \geqslant 10\,\mu$A. At 2 K, the residual resistance can be reduced by increasing the bias current [Fig. 2(b)]. The temperature dependence of resistance may be a signature of the single-particle tunneling in vertical transport process [28–31]. The phonon assistant tunneling is similar with the thermal activation mechanism. We then transform the R-T curves into Arrhenius plots ln$R$-1/T [Fig. 2(c)]. The data can be fitted by $R \sim e^{\Delta_b/k_B T}$ in the temperature range of 7–12 K, where Δ_b is the transport barrier height, k_B is Boltzmann's constant [32,33]. The fitting results give $\Delta_b \sim$ 0.87 and 0.082 meV for $I = 1$ and 60 μA, respectively, indicating the bias current reduced Δ_b. The ln$R$ versus $1/T$ curves deviate from the linear relation as temperature below 7 K.

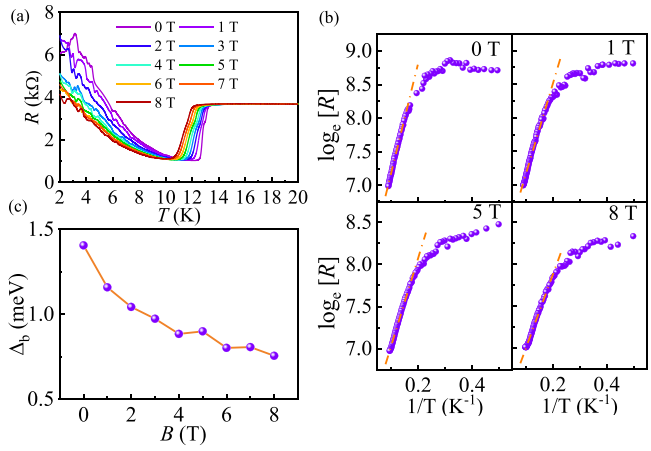

FIG. 3. (a) Temperature dependence of junction resistance of device B under various magnetic fields from 0 to 8 T. The junction resistance is reduced with increasing magnetic field below 10 K. (b) The Arrhenius plots of ln$R$ vs $1/T$ under different magnetic fields. The linear regimes are fitted to obtain the transport barrier height Δ_b. (c) The Δ_b as a function of magnetic field.

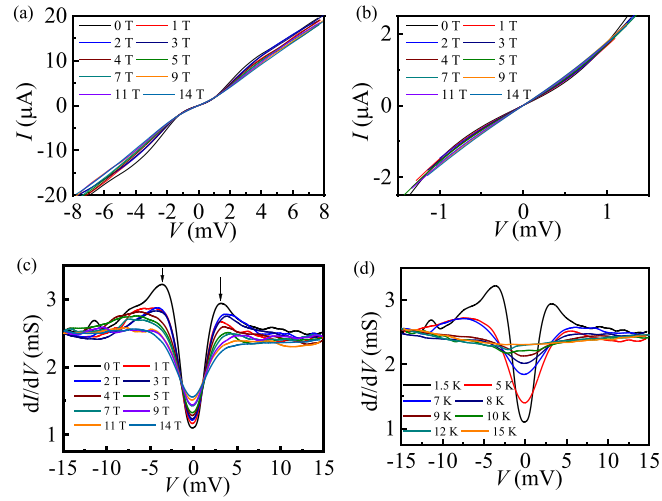

FIG. 4. (a) I-V curves under different magnetic fields of a NbN/$MoTe_2$/NbN vertical junction (device C). Excess current can be clearly observed. (b) I-V curves within small bias voltages (eV $<\Delta$). (c) The differential conductance at $T = 1.5$ K under different magnetic fields. A superconducting gap of 1.67 meV ($4\Delta =$ 6.66 meV as labeled by two arrows) is observed. (d) The differential conductance spectra at different temperatures from 1.5 to 15 K under zero magnetic field. The superconducting gap disappears at T above 10 K.

For pristine T_d-$MoTe_2$ sample, the onset of superconductivity is at ∼0.1 K [13]. Thus, the resistance drops shown in Fig. 2(a) should be related to the superconducting proximity effect of the Josephson junction. Residual resistance is presented in our all tested devices, indicating the low interfacial transparency between the Weyl semimetal $MoTe_2$ and the superconductor NbN in the devices [Fig. 2(d)] [34]. The resistance of top/bottom electrodes (R_m) as a function of temperature is displayed in Fig. 2(e), showing almost zero resistance below 13 K. Therefore, the measured residual resistance indicates the relatively weak superconducting proximity effect in the vertical junction. When an external magnetic field is applied, it can penetrate the NbN electrodes via vortex structures and interact with the $MoTe_2$ [21–23]. Figure 2(f) shows the MR of the NbN-$MoTe_2$-NbN vertical junction. The external magnetic field was applied perpendicular to the device surface and parallel with the vertical current. A negative MR behavior was observed with magnetic field up to 8 T (∼−16% at 2 and 5 K), which disappears at 15 K. Such negative MR behavior is unusual in conversional Josephson junctions [28–31], since the external magnetic field usually impedes the electron-electron pairing, which inevitably leads to the rising of resistance [29]. Considering $MoTe_2$ as a type-II Weyl semimetal, there exist many causes that would induce negative MR. However, it is worth noting that the negative MR only emerges within the superconducting regime. Thus, the current jetting effect or chiral anomaly [7] is unlikely the origin of such negative MR.

To further investigate the nature of the negative MR, we analyze the R-T curves of device B under various magnetic fields. The applied current is fixed at 0.1 μA. The R above T_c is almost irrelevant to magnetic field [Fig. 3(a)]. However, below 10 K, the junction resistance is clearly reduced with increasing magnetic field [Fig. 3(a)], indicating that the negative MR is from the N-S interface. The negative MR reaches ∼−48% under 8 T at 3 K. We convert the R-T curves into the Arrhenius plots of ln$R$ vs $1/T$ for different magnetic fields. The linear regimes are fitted by the relation $R \sim e^{\Delta_b/k_BT}$ [Fig. 3(b)], and the transport barrier height Δ_b is obtained. It is found that Δ_b is reduced by increasing magnetic field [Fig. 3(c)].

We further measured the I-V characteristics and differential conductance of an NbN/$MoTe_2$/NbN vertical junction (device C). The I-V curves under different magnetic fields are shown in Fig. 4(a). Excess current could be obtained by extrapolating the linear I-V trace when the voltage is larger than the superconductivity gap, which is attributed to the presence of Andreev reflections [28]. Reduced excess current by magnetic field is also observed in Fig. 4(a). The reduced excess current may be due to the magnetic field suppressed superconducting gap. Interestingly, the slopes of I-V curves at small biases is enhanced by magnetic fields, which in fact also reflects the negative MR since the slope reflects the conductance. As shown in Figs. 4(a) and 4(b), it could be found that the negative MR only emerges within the low bias regime. Under high bias, the slopes of I-V curves are hardly affected by magnetic fields. Figure 4(c) displays the dI/dV at $T = 1.5$ K under different magnetic fields from 0 to 14 T. A superconducting gap of 1.67 meV is observed [$4\Delta =$ 6.66 meV as labeled in Fig. 4(c)]. The factor 4 originates from the existence of two S-N interfaces in series [35]. Such a gap value corresponds to the gap of NbN electrodes (Δ is estimated at about 1.97 meV with $T_c \sim 13$ K). The zero-bias conductance is significantly enhanced by magnetic fields, which is enhanced by ∼41.6% under 14 T [Fig. 4(c)]. With increasing voltages, the differential conductance gradually increases, corresponding to the increase of Andreev reflection probability [34]. The dI/dV at different temperatures is shown in Fig. 4(d). The superconducting gap disappears above 10 K. Subharmonic gap structure, referring to a series of differential resistance peaks at $(\frac{2\Delta}{e})/n$ ($n = 1, 2, 3\ldots$), which is usually

related to multiple Andreev reflections [36], is absent in the *dI/dV* curves, indicating the low Andreev reflection probability within the low-bias voltages.

IV. DISCUSSION

Detailed investigations have been carried out in the Weyl semimetal $MoTe_2$ based vertical Josephson junctions. The magnetic field modulates the junction properties and results in the main observations: (i) enhanced zero-bias conductance by magnetic field below the critical temperature, (ii) negative MR that emerges as the system is in the superconductivity state and is within the low-bias voltages, and (iii) reduced transport barrier height and excess current by magnetic field. A natural explanation for magnetic field enhanced zero-bias conductance is that the superconducting proximity effect is suppressed by magnetic fields. Thus, the density of in-gap states may increase and lead to the increaseme of differential conductance in the conductance spectra at the low-bias region. In fact, the suppressed superconductivity might also explain the negative MR. The vertical junction in this case is regarded as a low transparency *SNS* junction. The conductance of the junction satisfies $\sigma_{NS} \propto \mathcal{T}^2/(2-\mathcal{T})^2$ under zero magnetic field [37], where $\mathcal{T}$ is the tunnel probability. With high barriers, $\mathcal{T}$ would be small. Thus, σ_{NS} is approximately proportional to the square of $\mathcal{T}$ and is expected to be small. However, when an external magnetic field is applied, the superconductivity could be poisoned. As the superconductivity is gradually removed by increasing magnetic field, the dependence of conductance on $\mathcal{T}$ is gradually changed from $\sigma_{NS} \propto \mathcal{T}^2$ to $\sigma_{NN} \propto \mathcal{T}$. As $\mathcal{T}$ is small, the enhanced conductance (i.e., the negative MR) would be expected. Based on present experimental results, we expect a further developed transport theory of the Weyl semimetal-based Josephson junctions elsewhere.

V. CONCLUSION

In summary, we have fabricated the vertical $NbN/MoTe_2/NbN$ junctions and investigated the transport properties as varying the temperature, magnetic field, and applied bias. Magnetic field enhanced zero-bias differential conductance is obtained. Negative MR is also observed as the system is in the superconducting regime. The magnetic field modulated interfacial properties between Weyl semimetal and superconductor should be valuable for further revealing the topological superconductivity and Majorana fermions in such a system.

ACKNOWLEDGMENTS

This work was supported by National Key Research and Development Program of China (Grants No. 2018YFA0703703 and No. 2016YFA0300802), and National Natural Science Foundation of China (Grants No. 91964201, No. 61825401, and No. 11774004).

Z.L., H.-D.S. and X.-G.Y. contributed equally to this work.

[1] M. N. Ali, J. Xiong, S. Steven Flynn, J. Tao, Q. D. Gibson, L. M. Schoop, L. Tian, N. Haldolaarachchige, M. Hirschberger, N. P. Ong, and R. J. Cava, Nature (London) **514**, 205 (2014).

[2] J. Tang, C. Zhang, D. Wong, Z. Pedramrazi, H. Tsai, C. Jia, B. Moritz, M. Claassen, H. Ryu, S. Kahn, J. Jiang, H. Yan, M. Hashimoto, D. Lu, R. G. Moore, C. C. Hwang, C. Hwang, Z. Hussain, Y. Chen, M. M. Ugeda *et al.*, Nat. Phys. **13**, 683 (2017).

[3] S. Wu, V. Fatemi, Q. D. Gibson, K. Watanabe, T. Taniguchi, R. J. Cava, and P. J. Herrero, Science **359**, 76 (2018).

[4] S. Y. Xu, Q. Ma, H. Shen, V. Fatemi, S. Wu, T. R. Chang, G. Chang, A. M. M. Valdivia, C. K. Chan, Q. D. Gibson, J. Zhou, Z. Liu, K. Watanabe, T. Taniguchi, H. Lin, R. J. Cava, L. Fu, N. Gedik, and P. J. Herrero, Nat. Phys. **14**, 900 (2018).

[5] Y. Y. Lv, X. Li, B. B. Zhang, W. Y. Deng, S. H. Yao, Y. B. Chen, J. Zhou, S. T. Zhang, M. H. Lu, L. Zhang, M. Tian, L. Sheng, and Y. F. Chen, Phys. Rev. Lett. **118**, 096603 (2017).

[6] Z. Wang, D. Gresch, A. A. Soluyanov, W. Xie, S. Kushwaha, X. Dai, M. Troyer, R. J. Cava, and B. A. Bernevig, Phys. Rev. Lett. **117**, 056805 (2016).

[7] A. A. Soluyanov, D. Gresch, Z. Wang, Q. S. Wu, M. Troyer, X. Dai, and B. A. Bernevig, Nature (London) **527**, 495 (2015).

[8] Y. Sun, S. C. Wu, M. N. Ali, C. Felser, and B. Yan, Phys. Rev. B **92**, 161107(R) (2015).

[9] D. H. Keum, S. Cho, J. H. Kim, D. H. Choe, H. J. Sung, M. Kan, H. Kang, J. Y. Hwang, S. W. Kim, H. Yang, K. J. Chang, and Y. H. Lee, Nat. Phys. **11**, 482 (2015).

[10] L. Huang, T. M. McCormick, M. Ochi, Z. Zhao, M. T. Suzuki, R. Arita, Y. Wu, D. Mou, H. Cao, J. Yan, N. Trivedi, and A. Kaminski, Nat. Mater. **15**, 1155 (2016).

[11] J. Jiang, Z. K. Liu, Y. Sun, H. F. Yang, C. R. Rajamathi, Y. P. Qi, L. X. Yang, C. Chen, H. Peng, C. C. Hwang, S. Z. Sun, S. K. Mo, I. Vobornik, J. Fujii, S. S. P. Parkin, C. Felser, B. H. Yan, and Y. L. Chen, Nat. Commun. **8**, 13973 (2017).

[12] X. Luo, F. C. Chen, J. L. Zhang, Q. L. Pei, G. T. Lin, W. J. Lu, Y. Y. Han, C. Y. Xi, W. H. Song, and Y. P. Sun, Appl. Phys. Lett. **109**, 102601 (2016).

[13] Y. Qi, P. G. Naumov, M. N. Ali, C. R. Rajamathi, W. Schnelle, O. Barkalov, M. Hanfland, S. C. Wu, C. Shekhar, Y. Sun, V. Süβ, M. Schmidt, U. Schwarz, E. Pippel, P. Werner, R. Hillebrand, T. Förster, E. Kampert, S. Parkin, R. J. Cava *et al.*, Nat. Commun. **7**, 11038 (2016).

[14] Z. Guguchia, F. von Rohr, Z. Shermadini, A. T. Lee, S. Banerjee, A. R. Wieteska, C. A. Marianetti, B. A. Frandsen, H. Luetkens, Z. Gong, S. C. Cheung, C. Baines, A. Shengelaya, G. Taniashvili, A. N. Pasupathy, E. Morenzoni, S. J. L. Billinge, A. Amato, R. J. Cava, R. Khasanov, and Y. J. Uemura, Nat. Commun. **8**, 1082 (2017).

[15] Y. Li, Q. Gua, C. Chen, J. Zhang, Q. Liu, X. Hua, J. Liu, Y. Liua, L. Ling, M. Tiang, Y. Wang, N. Samarth, S. Lid, T. Zhang, J. Feng, and J. Wang, Proc. Natl. Acad. Sci. USA **115**, 9503 (2018).

[16] A. Chubukov, Annu. Rev. Condens. Matter Phys. **3**, 57 (2012).

[17] N. Bovenzi, M. Breitkreiz, P. Baireuther, T. E. O'Brien, J. Tworzydło, İ. Adagideli, and C. W. J. Beenakker, Phys. Rev. B **96**, 035437 (2017).
[18] H. Zhang, C. X. Liu, S. Gazibegovic, D. Xu, J. A. Logan, G. Wang, N. Loo, J. D. S. Bommer, M. W. A. Moor, D. Car, R. L. M. Op het Veld, P. J. Veldhoven, S. Koelling, M. A. Verheijen, M. Pendharkar, D. J. Pennachio, B. Shojaei, J. S. Lee, C. J. Palmstrøm, E. P. A. M. Bakkers *et al.*, Nature (London) **556**, 74 (2018).
[19] Ö. Gül, H. Zhang, J. D. S. Bommer, M. W. A. de Moor, D. Car, S. R. Plissard, E. P. A. M. Bakkers, A. Geresdi, K. Watanabe, T. Taniguchi, and L. P. Kouwenhoven, Nat. Nanotechnol. **13**, 192 (2018).
[20] P. San-Jose, E. Prada, and R. Aguado, Phys. Rev. Lett. **112**, 137001 (2014).
[21] M. Beck, M. Klammer, S. Lang, P. Leiderer, V. V. Kabanov, G. N. Gol'tsman, and J. Demsar, Phys. Rev. Lett. **107**, 177007 (2011).
[22] M. P. Mathur, D. W. Deis, and J. R. Gavaler, J. Appl. Phys. **43**, 3158 (1972).
[23] Y. Noat, V. Cherkez, C. Brun, T. Cren, C. Carbillet, F. Debontridder, K. Ilin, M. Siegel, A. Semenov, H. W. Hübers, and D. Roditchev, Phys. Rev. B **88**, 014503 (2013).
[24] T. Georgiou, R. Jalil, B. D. Belle, L. Britnell, R. V. Gorbachev, S. V. Morozov, Y. J. Kim, A. Gholinia, S. J. Haigh, O. Makarovsky, L. Eaves, L. A. Ponomarenko, A. K. Geim, K. S. Novoselov, and A. Mishchenko, Nat. Nanotechnol. **8**, 100 (2013).
[25] L. Fu and C. L. Kane, Phys. Rev. Lett. **100**, 096407 (2008).
[26] C. Z. Li, C. Li, L. X. Wang, S. Wang, Z. M. Liao, A. Brinkman, and D. P. Yu, Phys. Rev. B **97**, 115446 (2018).
[27] M. B. Shalom, M. J. Zhu, V. I. Fal'ko, A. Mishchenko, A. V. Kretinin, K. S. Novoselov, C. R. Woods, K. Watanabe, T. Taniguchi, A. K. Geim, and J. R. PranceShalom, Nat. Phys. **12**, 318 (2016).
[28] G. E. Blonder, M. Tinkham, and T. M. Klapwijk, Phys. Rev. B **25**, 4515 (1982).
[29] R. J. Soulen Jr., J. M. Byers, M. S. Osofsky, B. Nadgorny, T. Ambrose, S. F. Cheng, P. R. Broussard, C. T. Tanaka, J. Nowak, J. S. Moodera, A. Barry, and J. M. D. Coey, Science **282**, 85 (1998).
[30] K. Y. Yang, K. Huang, W. Q. Chen, T. M. Rice, and F. C. Zhang, Phys. Rev. Lett. **105**, 167004 (2010).
[31] R. Meservey and P. Tedrow, Phys. Rep. **238**, 173 (1994).
[32] L. Zhang, Y. Yan, H. C. Wu, D. Yu, and Z. M. Liao, ACS Nano **10**, 3816 (2016).
[33] L. Britnell, R. V. Gorbachev, R. Jalil, B. D. Belle, F. Schedin, A. Mishchenko, T. Georgiou, M. I. Katsnelson, L. Eaves, S. V. Morozov, N. M. R. Peres, J. Leist, A. K. Geim, K. S. Novoselov, and L. A. Ponomarenko, Science **335**, 947 (2012).
[34] L. Maier, J. B. Oostinga, D. Knott, C. Brüne, P. Virtanen, G. Tkachov, E. M. Hankiewicz, C. Gould, H. Buhmann, and L. W. Molenkamp, Phys. Rev. Lett. **109**, 186806 (2012).
[35] Y. J. Doh, J. A. Dam, A. L. Roest, E. P. A. M. Bakkers, L. P. Kouwenhoven, and S. D. Franceschi, Science **309**, 272 (2005).
[36] M. Octavio, M. Tinkham, G. E. Blonder, and T. M. Klapwijk, Phys. Rev. B **27**, 6739 (1983).
[37] C. W. J. Beenakker, Phys. Rev. B **46**, 12841 (1992).